Extraction of mode mixity and other fracture data from crack paths in pull-off adhesion tests

Heather P. H. Liddell[a,], Gregory M. Smith[b], and Laura Erickson[c]*

[a]American Society for Engineering Education – U.S. Naval Research Laboratory (ASEE-NRL)
[b]Center for Corrosion Science and Engineering, Code 6138, U.S. Naval Research Laboratory
[c]Rampart, LLC
Washington, D.C., 20375, USA
[*]heather.liddell.ctr@nrl.navy.mil

Introduction

In a standard pull-off adhesion test (ASTM D4541), illustrated in Figure 1, a pull stub is attached to a coated substrate and then removed through vertical loading. The force required to separate the coating from its substrate provides a measure of its adhesion strength. While pull-off adhesion tests provide a convenient, standardized, and rapid technique for evaluating the adhesion strength of a paint or coating, these tests have not generally provided the basis for a deeper fracture mechanics understanding. Yet visual examinations of used pull stubs reveal predictable, characteristic fracture patterns for like coating systems. This suggests a missed opportunity to analyze such crack "signatures" for further insight into fracture processes.

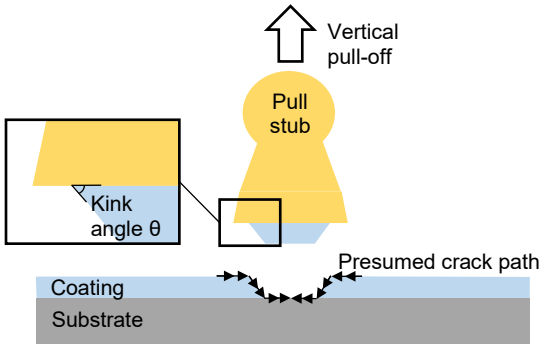

This talk will explore two methods for extracting analytically useful data from used adhesion test stubs, which are normally simply discarded. First, we present a technique for back-calculating the mode mixity of fracture from experimental measurements of the crack path (specifically, the crack kink angle θ). This technique provides the powerful capability to disambiguate mode I / mode II fracture post hoc, without prior knowledge of loading conditions. Second, we apply a machine-learning-based image segmentation tool (Trainable WEKA [1]) to inspect and quantify the fractional area coverage of coating layer(s) on used pull stubs, providing insight into the roles of each material in the fracture process. These simple-to-use techniques demonstrate a substantial enhancement in the richness of data available from pull-off adhesion tests.

Materials

Three epoxy-based coating systems were tested:

- **Coating A:** an epoxy novolac amine system (98% solids) with an average thickness of 470 µm;
- **Coating B:** an epoxy polyamide system (67% solids), applied in two layers, with an average total thickness of 231 µm; and
- **Coating AB:** a two-layer system consisting of a base layer of Coating A and a topcoat of Coating B, with a combined average thickness of 696 µm.

Material properties are shown in Table 1. Coatings were deposited onto steel substrates having dimensions of 152 mm x 305 mm x 6 mm (6" x 12" x 1/4") and cured according to manufacturer recommendations. After curing, coated panels were lightly scuff-sanded and 20-mm aluminum dolly pull stubs (DeFelsko Inspection Instruments) were affixed to the coated surfaces using a two-part epoxy adhesive. The minimum center-to-center spacing between adjacent stubs was 51 mm (2 inches). In total, 144 pull stubs (48 stubs per coating, 12 stubs per panel) were analyzed.

Table 1. Material properties of coatings and pull stubs: elastic modulus E, Poisson's ratio ν, and shear modulus μ

	E (GPa)	ν	μ (GPa)
Coating A (epoxy novolac amine)	1.75	0.31	0.67
Coating B (epoxy polyamide)*	1.65	0.35	0.61
Pull stub (aluminum)	69.0	0.30	26.5

* Coating B was treated as a single layer system, since the primer and topcoat had nearly identical mechanical properties.

Microscopy of Adhesion Pull Stubs

Each used pull stub was imaged in two orientations. Top-down micrographs, which allowed visualization of the coating removal pattern and failure interfaces, were captured using a Nikon SMZ 1500 stereo microscope. Four quadrant micrographs were stitched together to generate a

complete composite image of each 20-mm-diameter pull stub. Side-on micrographs, which allowed visualization of the crack path and measurement of the crack angle, were captured using a horizontally mounted Navitar 12x zoom lens. Figure 2 shows representative images in each view.

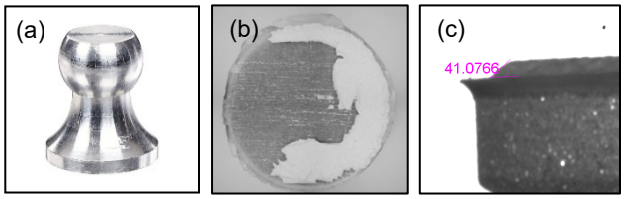

Figure 2. A 20-mm-diameter pull stub [photo in (a)], imaged in (b) top-down and (c) side-on orientations.

Prediction of Mode Mixity from Crack Path

For the fracture mechanics model, we assumed a crack that begins at the outer perimeter of the pull stub. If energetically favorable, the crack may propagate initially along the coating/stub interface, but in most cases (excepting cases of "glue failure"), the crack eventually kinks downward through the coating at angle θ, and a portion of the coating is removed with the stub, as depicted in Figure 1.

He and Hutchinson [2] showed that for an interfacial crack between dissimilar media, the ratio of the energy release rate for a kinked crack, G, and that of a crack advancing in the interface, G_0, is given by equation (1):

$$\frac{G}{G_0} = \frac{|c|^2 + |d|^2 + 2\,\mathbf{Re}[cd\exp(2i\bar{\psi})]}{\sqrt{(1-\beta^2)/(1+\alpha^2)}}, \qquad (1)$$

where α and β are the Dundurs material-mismatch parameters, which depend on the shear moduli (μ_1, μ_2) and Poisson's ratios (ν_1, ν_2) of the interfacing materials:

$$\alpha = \frac{\mu_1(1-\nu_2) - \mu_2(1-\nu_1)}{\mu_1(1-\nu_2) + \mu_2(1-\nu_1)}; \qquad (2)$$

$$\beta = \frac{1}{2}\left[\frac{\mu_1(1-2\nu_2) - \mu_2(1-2\nu_1)}{\mu_1(1-\nu_2) + \mu_2(1-\nu_1)}\right]. \qquad (3)$$

The mode-mixity angle ψ describes the crack loading, and is defined as $\psi = \tan^{-1}(K_{II}/K_I)$, where K_I and K_{II} are the mode-I (opening) and mode-II (shearing) stress intensity factors, respectively. The corrected mode-mixity $\bar{\psi}$ appearing in equation (1) is adjusted for the problem length scale as $\bar{\psi} = \psi + \varepsilon \ln(a/h)$, where a is the crack length, h is the coating thickness, and ε is the bimaterial constant given by

$$\varepsilon = \frac{1}{2\pi}\ln\left(\frac{1-\beta}{1+\beta}\right). \qquad (4)$$

The quantities c and d in equation (1) are complex-valued functions that depend on α, β, and θ, and have been tabulated by He and Hutchinson as a function of θ [3].

Based on equation (1), we can express G/G_0 as a function of crack kink angle θ for any mode-mixity angle ψ. When $G/G_0 > 1$, the crack will prefer to kink into the coating rather than continuing along the interface. If a local maximum of G/G_0 exists for a non-zero value of θ, we interpret this as an energetically favorable kink angle. Thus, if loading conditions (and thus the mode-mixity angle ψ) are known, we can calculate the preferred kink angle by identifying the maximum of the G/G_0 curve. Conversely, if experimental measurements of crack kink angles are known, we can back out an estimate of the mode-mixity angle ψ by assuming fracture consistent with the most energetically favorable crack path. A similar approach was taken in Ref. 4.

With well-known loading conditions, the conventional ASTM D4541 adhesion test provides an ideal case for experimental validation of this analytical technique (which could then be extended to situations for which loading conditions are uncertain). Modeling the stub/coating system as a bilayer held between rigid grips, we estimated the mode-mixity angle $\psi(\alpha,\beta)$ by interpolating over Hutchinson and Suo's numerical data [5]. We corrected for length scale by assuming a crack length a equal to the thickness of the coating layer in which the crack advanced, and a coating thickness h equal to the thickness of the overall coating stack ahead of the crack. The calculated mode-mixity angles $\psi(\alpha,\beta)$, length scales a/h, and corrected mode-mixity angles $\bar{\psi}(\alpha,\beta)$ are shown in Table 2.

Table 2. Mode-mixity angles and length-scale corrections for each material interface

System	Interface	$\psi(\alpha,\beta)$	a/h	$\bar{\psi}(\alpha,\beta)$
A	Stub to A	15.0°	1	15.0°
B	Stub to B	18.4°	1	18.4°
AB	Stub to B	18.4°	0.33	22.9°
AB	A to B	16.2°	1	16.2°

Figure 3.

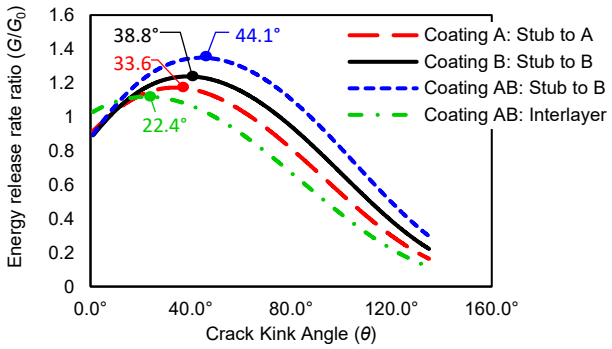

Figure 3. Energy release rate ratio G/G_0 plotted as a function of crack kink angle θ, annotated with the energetically preferred crack kink angle θ_p for each material interface

Analytical predictions of θ_p are compared to experimental measurements of crack kink angle in Table 3. Each experimental data point reflects the average of between 231 and 323 angle measurements. Several measurements were made on each stub, each representing a different location on

the stub, with 48 stubs measured in total for each coating. Results of this comparison are promising. Experimental crack kink angles were within 1% to 25% of analytical predictions for the four cases examined. This consistency demonstrates strong potential for this technique as a way to "convert" between mode mixity and crack kink angle.

Table 3. Analytically predicted and experimentally measured crack kink angles for the four interfaces studied

System	Interface	Analytical θ_p	Experimental θ_m avg. ± S.D.	n
A	Stub to A	33.6°	31.7° ± 7.6°	311
B	Stub to B	38.8°	34.5° ± 11.6°	231
AB	Stub to B	44.1°	44.7° ± 8.3°	269
AB	A to B	22.4°	28.0° ± 8.2°	323

Fracture Analysis via Image Segmentation

Since ASTM D4541 requires pull-to-failure, fracture necessarily propagates across the entire stub—but failure might occur at any combination of materials and interfaces. Clearly, fracture at certain interfaces is more problematic than at others. For example, if fracture most frequently occurs at the substrate, resulting in a large portion of the coating being removed with the pull stub, this might suggest a coating susceptible to catastrophic delamination. Image segmentation allows us to quantitatively assess and compare the most likely failure interfaces for a given coating.

To quantify the fractional area occupied by each material on the pull stubs, Trainable WEKA (a machine-learning-based image segmentation plug-in for ImageJ [1]) was deployed. A custom "classifier" was trained for each coating system, iterating on multiple training images until accurate segmentation of an arbitrary image was demonstrated. Trained classifiers were then applied in a batch process to segment all images. Figure 4 shows examples of original and segmented images for each coating systems.

Image segmentation results are shown in Table 4 for the three coating systems considered here. Fracture patterns that include high area fractions for *adhesive* and *aluminum stub* are considered the best outcomes, since in those regions, the coating remained intact and adhered to the substrate panel. Fracture patterns that include high area fractions for the *coating* indicate inferior performance, since at least some of the coating was lifted from the panel with the stub.

Table 4. Image segmentation results: average fractional area coverage of each material on used pull stubs

	Coating system		
	A	**B**	**AB**
Coating	45.2%	31.7%	91.0%
Adhesive	52.9%	10.3%	0.0%
Aluminum stub	1.8%	57.9%	9.0%

For the material systems considered here, coating removal represented an average of 32%, 45%, and 91% of stub area for Coatings B, A, and AB respectively, suggesting that Coating B offered the most desirable fracture pattern. This visually driven assessment provides a useful accompaniment to ASTM D4541 adhesion test data, particularly for coatings that yield similar adhesion strengths. Indeed, this was the case for the coatings considered here: all three coatings performed nearly identically in adhesion strength testing (differences were not statistically significant), but nonetheless could be clearly ranked by desirability of the typical failure pattern.

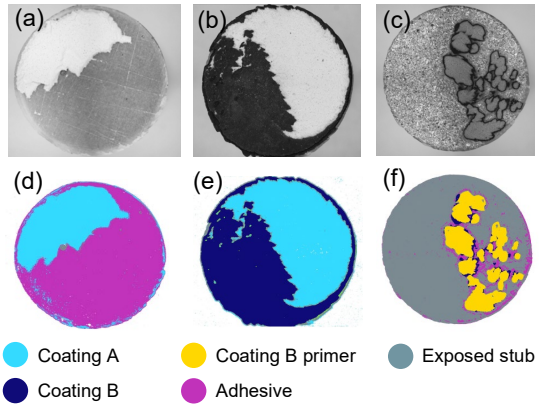

Figure 4. Examples of stub micrographs and corresponding image segmentation results for Coating A (a,d), Coating AB (b,e), and Coating B (c,f).

Conclusions

Here we demonstrated two new methods for extracting fracture data from used pull-off adhesion test stubs, which are normally discarded. The technique for estimating mode mixity from crack kink angle enables disambiguation of mode-I and mode-II fracture post hoc, which is quite powerful. While the loading conditions are known in a standard ASTM D4541 adhesion test, the technique can be extended to situations where the loading conditions are unknown or uncertain. For example, this technique is now being used in our laboratory to develop and validate modified adhesion tests that incorporate mixed-mode loading, and has potential for use in forensic failure analysis of delamination defects. The second technique, image segmentation and analysis, provides a way to quantify the most likely failure interfaces for a given coating. This assessment complements adhesion strength data, and enables objective comparisons across coating systems that yield similar adhesion strengths.

References

1. I. Arganda-Carreras, V. Kaynig, C. Ruedon, et al., *Bioinformatics*, 2017, 33, pp. 2424-2426.
2. M.-Y. He and J. W. Hutchinson, *J. Appl. Mechanics*, 1989, 56, pp. 270-278.
3. M.-Y. He and J. W. Hutchinson, Technical Report MECH-113A (Harvard University, 1989).
4. H. P. H. Liddell, K. Mehrotra, et al., *Applied Optics*, 2013, 52, pp. 7689-7698
5. J. W. Hutchinson and Z. Suo, *Advances in Applied Mechanics*, 1992, 29, pp. 63-191